JOURNAL OF COMPUTATIONAL PHYSICS 119, 356–373 (1995)

Electromagnetic Scattering from Dielectrically Coated Axisymmetric Objects Using the Generalized Point-Matching Technique (GPMT)

II. Numerical Results and Comparisons

H. M. AL-RIZZO and J. M. TRANQUILLA

Radiating Systems Research Laboratory, Electrical Engineering Department, University of New Brunswick, Fredericton, New Brunswick, Canada

Received May 25, 1994

In Part I, the theoretical formulation of a numerical solution to electromagnetic scattering problems encompassing arbitrarily oriented, three-dimensional axisymmetric perfectly conducting or dielectric objects embedded in an axisymmetric dielectric obstacle has been developed in a form suitable for an efficient computer solution. Here, numerical results for a wide variety of scatterer configurations are presented in order to demonstrate the validity and accuracy of our generalized point-matching technique formulation. Whenever possible, the Mie theory, the extended Mie theory, the homogeneous extended boundary-condition method (EBCM), the multilayered EBCM, and the Rayleigh–Gans–Debye approximation have been used in the process of examining the applicability of the suggested method. In all of the cases considered, excellent agreement has been achieved.

I. INTRODUCTION

Using the analytical formulation presented in [1], a versatile computer program has been developed in FORTRAN 77 for the HP-UX 8000 computer. For a given scattering geometry, the expansion coefficients of the spherical vector wavefunction expansions for the internal and scattered field vectors, the angular scattering patterns, and the various cross sections of interest are evaluated for two principal orthogonally polarized components of the incident field vector. The programs have been configured to produce solutions to electromagnetic (EM) scattering problems involving either axisymmetric homogeneous perfectly conducting (PC) or dielectric scatterers or PC or dielectric obstacles embedded in a dielectric coating, both with and without a plane of symmetry perpendicular to their axis of rotational symmetry. In order to obtain a satisfactorily correct solution for a given scatterer in an arbitrary orientation, a sufficient number of terms must be incorporated into the truncated expansions of the internal and scattered field vectors, depending on the desired accuracy. Since computational time is directly related to the length of the expansions to be included, it is essential to devise an algorithm whereby the minimum upper modal indices M_0 and N_0, which are not known a priori, required for a satisfactory convergence can be determined reliably. Excess azimuthal and/or elevation modes are capable of degrading the convergence and should be avoided as they may introduce errors in the final solution, especially if they are inaccurately computed.

The scheme followed for the determination of the minimum upper modal indices M_0 and N_0 is similar to the one implemented by Barber and Hill [4] in their extended boundary condition method (EBCM) code and consists of two separate parts. First, the elevation θ_0 and azimuthal ϕ_0 orientation angles of the local frame are both set to zero; i.e., the case of an axial (nose-on) incidence, with no cross-polarized scattered wave being generated, is imposed. Therefore, only the aximuthal mode $m = 1$ is included and N_0 is then determined for this symmetric orientation, starting from an initial truncation estimate which is taken as the integer closest to $k_0a/2$, where a is a typical maximum linear dimension of the scatterer. Convergence is taken in the Cauchy sense; i.e., accuracy is based on the criterion of the relative constancy of the various scattering parameters when two successive elevation modal indices result in a specified percentage difference [7]. From our computational experience, it has been concluded that the number of significant elevation modal indices is determined mainly by the shape and size while it is weakly dependent on the constitutive parameters of the scatterer.

Once the truncation size N_0 has been determined, a general orientation, for which a cross-polarized component will be generated, is considered next by setting $\theta_0 = \phi_0 = 45°$. With n fixed at N_0, the number of significant azimuthal modes M_0 is similarly obtained. Although N_0 is the theoretical upper limit for m, it has been observed throughout the course of computations that convergence over the azimuthal modal index m can quite easily be achieved without necessarily summing over all the elevation model indices.

In all cases to be presented, the set of numerical results given has been obtained for a total number of boundary-matching

0021-9991/95 $12.00

points which is chosen at a given azimuthal modal index such that the total number of boundary-condition equations is overspecified by a factor of 2, i.e., $L_m = 2\{N_0 - m + 1 - \delta_{m0}\}$.

The majority of our graphical results describes the behavior of the differential scattering cross-section patterns, normalized by πa^2, where a is a characteristic dimension along the axis of rotational symmetry. Results evaluated from the generalized point-matching technique (GPMT) are displayed at one-sixth degree increments while those obtained from the EBCM [5] or Rayleigh–Gans–Debye (RGD) approximation [6] are computed at 10° intervals. For some selected cases, three fixed scatterer orientations have been considered, $\theta_0 = \phi_0 = 0°$, $\theta_0 = \phi_0 = 90°$, and $\theta_0 = \phi_0 = 45°$. Throughout this paper, the scattered electric field vector has been evaluated for two orthogonal polarization directions of the incident wave. In presenting the angular scattering results, the convention which has been followed is based on the fact that since, when no cross-polarized scattered wave is generated ($\theta_0 = \phi_0 = 0°$ and $\theta_0 = \phi_0 = 90°$), the co-polarized patterns which are mirror images about $\theta_s' = 180°$ are given for $0° \leq \theta_s' \leq 180°$. For $\theta_0 = \phi_0 = 45°$, a cross-polarized component exists and therefore the whole asymmetric patterns are consequently displayed. Unless otherwise stated, the scattering parameters as computed from the GPMT and the EBCM are accurate within at least 1%, which seemed to be appropriate for the cases to be presented, bearing in mind the high cost of accomplishing convergence if higher accuracies are demanded.

II. NUMERICAL RESULTS

1. *Homogeneous Scatterers*

The programs were first run for the simple case of lossy and lossless dielectric spherical scatterers [2] and certain parameters were varied to determine their effects on the results. However, by using a mathematical artifice, this initial evaluation has been extended to a nontrivial test whereby the expected levels of accuracy for homogeneous nonspherical scatterers can be inferred [8]. This is achieved by moving the origin of the local frame off center along the z-axis by a distance d ($-a < d < a$), where a is the radius of the sphere, and thus, mathematically, the scatterer appears to be nonspherical since the radius vector and its derivative with respect to the polar angle θ are now functions of the angle θ. As expected, the programs should provide the same far-field scattering solution irrespective of the value of d, and therefore the required increase in the number of elevation modal indices, because of this sufficiently general, nonmirror symmetric shape provides an indication of the convergence of the results when dealing with other general nonspherical scatterer shapes. A representative case of these calculations is displayed in Fig. 1.

The second geometry to be considered is that of the largest and, hence, the most eccentric, oblate spheroidal raindrop with an equivolumic radius of 3.25 mm and an axial ratio, $a/b = 0.675$, where a and b denote the length of the semi-minor and semi-major axes of the scatterer, respectively. The computations were performed for a raindrop temperature of 20° C and at a frequency of 300 GHz with a relative dielectric constant, $\varepsilon_r = 5.4384 + j4.2005$. The purpose of this test is twofold. First, the applicability of the GPMT to homogeneous lossy dielectric scatterers of large size parameters, $k_0 b = 23.28$, which were not previously considered, is demonstrated. Second, the capability of the GPMT to yield accurate scattering patterns, generated from an arbitrarily oriented scatterer, for both the co- and cross-polarized components is verified even for values at deep nulls, despite the fact that they are relatively very small numbers and, hence, are susceptible to computational roundoff errors. Typical results of our scattering computations are shown in Fig. 2. It is evident from the results of the lossy oblate spheroidal scatterer test that an excellent consistency between the results of the GPMT and the EBCM has been achieved where typical differences are less than 1%.

The next scatterer shape to be considered involves a homogeneous lossless dielectric prolate spheroid of relative dielectric constant, $\varepsilon_r = 2.25$. Typical scattering calculations are shown in Fig. 3 for $a/b = 2$ and for two size parameters, $k_0 a = 30$ and 37.699, which at a frequency of 30 GHz corresponds to a major axis length of 95.4929 mm and 120 mm, i.e. $2a = 14.3239\lambda$ and 15λ, where λ is the wavelength index of the dielectric object.

The excellent agreement attained thus far has led to the consideration of further assorted cases of axisymmetric scatterers which do not possess an equatorial plane of reflection symmetry. In the following, the scattering by the realistic raindrop shapes as derived by Pruppacher and Pitter [9] (P-P) will be considered. It is interesting to mention that Yeh *et al.* [10] claimed that of the different analytical and numerical scattering techniques available, only the EBCM and the finite element method (FEM) are capable of providing reliable results in the resonance region with little uncertainty. However, we have conducted extensive comparison tests between the GPMT and EBCM for scattering from P-P raindrops, the results of which reveal the important conclusion that, although the EBCM has been widely believed to be applicable to arbitrarily shaped dielectric scatterers of large volumes [11, 12], the numerical behavior of the EBCM degrades significantly when dealing with scattering geometries which do not possess a mirror symmetry in the direction of the normal to the axis of revolution. In fact our extensive numerical experience with the programs of Barber and Hill [4] showed that the EBCM was unable to provide a convergent solution over the entire scattering plane for a P-P raindrop with $a_0 = 3.25$ mm, where a_0 is the radius of a sphere with the same volume as the deformed P-P drop, at frequencies greater than about 6 GHz. The differential scattering characteristics of two P-P drops of equivolumic sizes $a_0 =$ 3 and 3.5 mm at frequencies of 6 and 33 GHz and for a raindrop temperature of 10° C are shown in Fig. 4. The first frequency

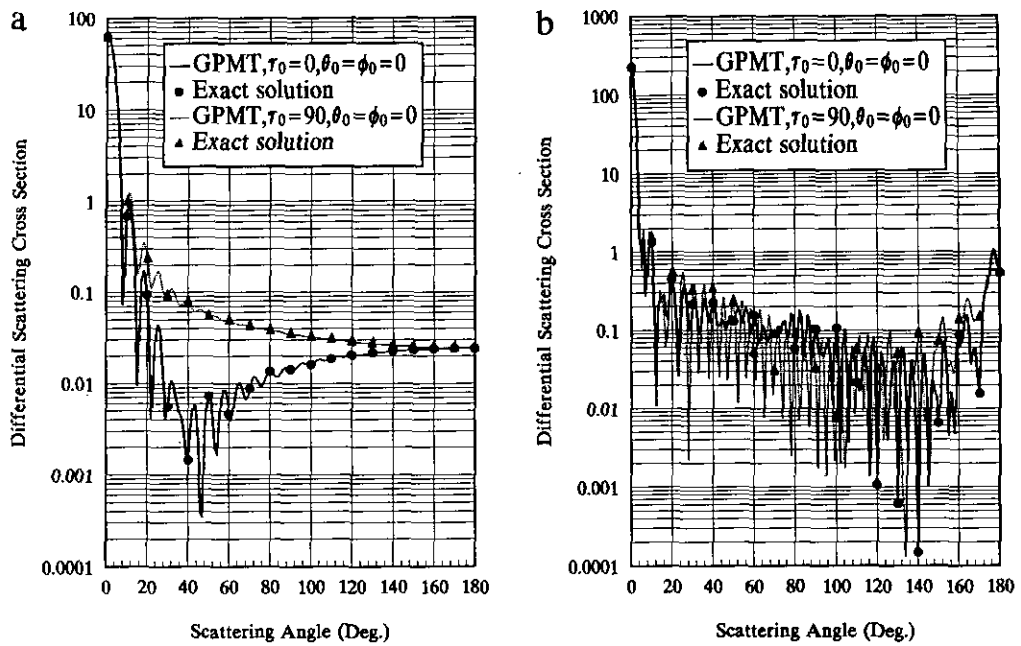

FIG. 1. Plots of normalized differential scattering cross-section patterns for displaced, homogeneous dielectric spherical scatterers: (a) k_0a = 25.1327, ε_r = 10 + j5, d/a = 0.4; (b) k_0a = 50.2654, ε_r = 5, d/a = 0.2.

was selected because of the ability of the EBCM to provide a convergent solution when a_0 = 3 mm while the second one has been chosen since it is the highest frequency for which Fang and Lee [13] have published tabulated results for the forward and backward scattering amplitude functions using the FEM. For comparison purposes, in Fig. 5 the amplitude and phase of the forward and backward scattering amplitude functions of the 13 P-P raindrops in a fixed orientation, θ_0 = ϕ_0 = 90°, obtained from the GPMT are displayed as a function of the equivolumic spherical raindrop radius in the range from 0.25

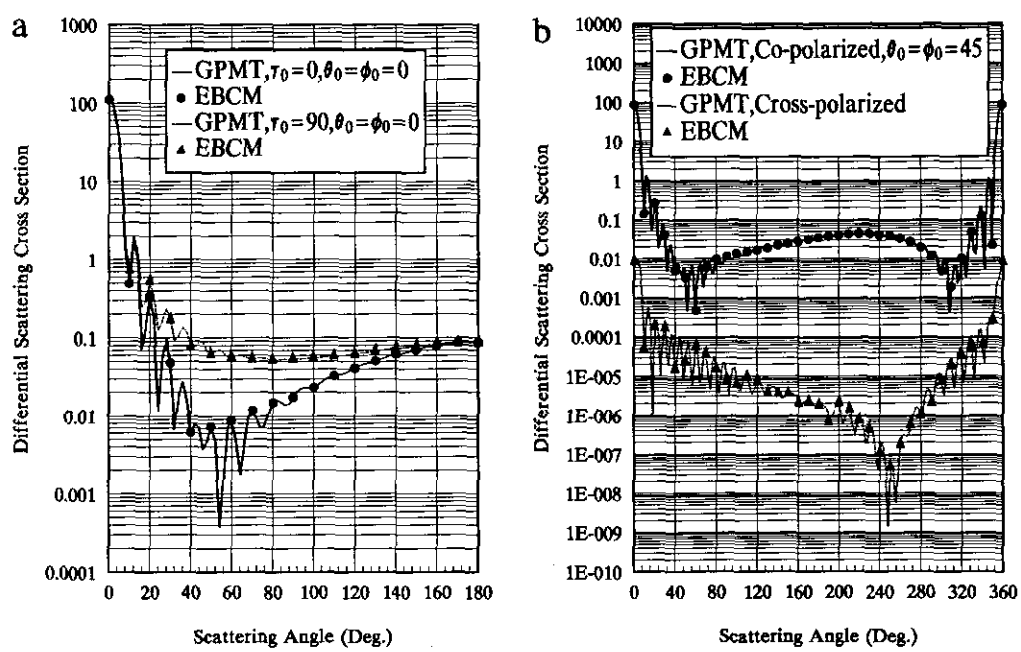

FIG. 2. Plots of normalized differential scattering cross-section patterns for an oblate spheroidal raindrop with an equivolumic spherical radius = 3.25 mm and axial ratio = 0.675 at a frequency of 300 GHz: (a) τ_0 = 0° and 90°; (b) τ_0 = 0°. Main (co-)polarization is parallel to the scattering (xz) plane.

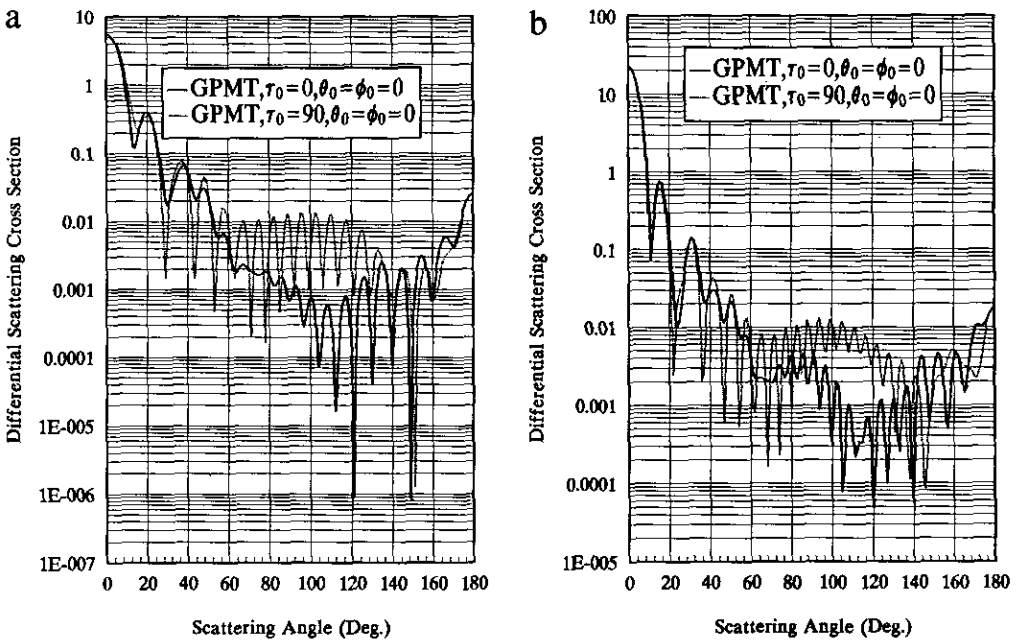

FIG. 3. Plots of normalized differential scattering cross-section patterns for lossless homogeneous prolate spheroidal scatterers with $\varepsilon_r = 2.25$: (a) $k_0a = 30$; (b) $k_0a = 37.699$.

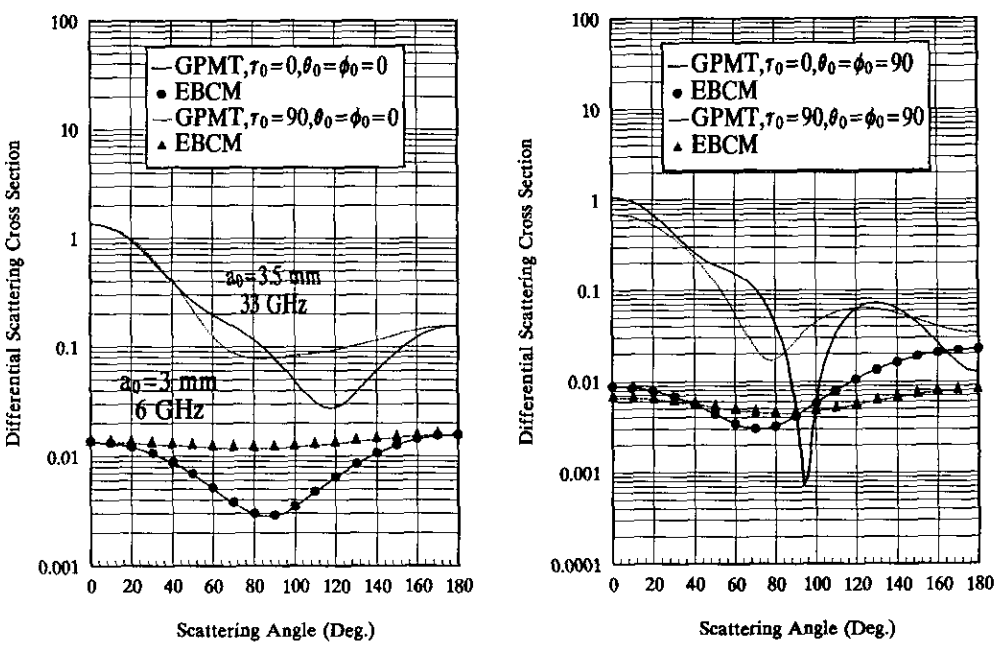

FIG. 4. Plots of normalized differential scattering cross-section patterns for two P-P raindrops with equivolumic spherical radii of 3 and 3.25 mm at frequencies of 6 and 33 GHz.

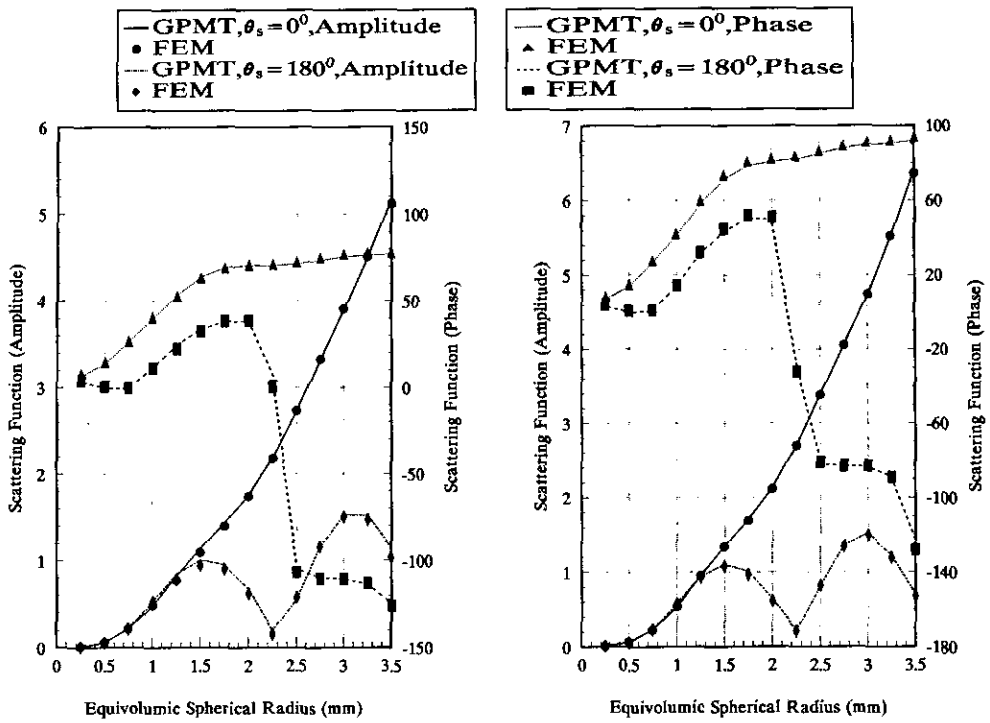

FIG. 5. Amplitude and phase of the forward and backward scattering amplitude functions of P-P raindrops as a function of the equivolumic radius, a_0 = 0.25 and 3.5 mm at frequencies of 33 GHz: (a) $\theta_0 = \phi_0 = 90°$, $\tau_0 = 90°$; (b) $\theta_0 = \phi_0 = 90°$, $\tau_0 = 0°$.

to 3.5 mm for parallel and perpendicular incident polarizations, along with the results of the FEM [13] at a frequency of 33 GHz and a raindrop temperature of 10° C, where a high degree of agreement is apparent for both the amplitude and the phase of the forward and backward scattering amplitude functions.

The final class of homogeneous nonspherical scatterers, which has received comparatively little attention in the literature [14, 15] involved Chebyshev particles. Mugani and Wiscombe [14] utilized the EBCM and Kiehl *et al.* [15] applied the first-order perturbation theory to investigate EM scattering from rotationally symmetric nonspherical Chebyshev particles with surfaces parameterized by

$$r(\theta) = a_0[1 + \Delta T_n \{\cos \theta\}], \tag{1}$$

where Δ is the deformation parameter ($|\Delta| < 1$), a_0 is the radius of the unperturbed sphere and $T_n\{\cos\theta\}$ is the nth-order Chebyshev polynomial.

As has been observed in the P-P raindrop scattering computations, we have also encountered consistently repeated numerical overflow problems in the EBCM with a convergence criterion of 1% no longer being achieved over 80% of 10 selected scattering angles, θ_s, in the range from 0° to 180°, particularly when the size parameter k_0a_0 exceeded about 10, even for particles with $n = 3$. Similarly Kiehl, *et al.* [15] found that the accuracy of the extinction efficiency evaluated from the first-order perturbation theory for $\Delta = 0.1$, $n = 2$ degraded significantly when $k_0a_0 > 6$. It should be mentioned that the convergence rate of the extinction efficiency is usually faster in both the GPMT and EBCM as compared to scattering in other directions. On the other hand, the GPMT which has not been previously employed to treat scattering by such particle shapes, was found to give very satisfactory numerical performance with excellent agreement being achieved with the cases that could be handled by the EBCM and it also provided a converged solution with a convergence criterion of 0.1% or better for cases in which it was not possible to achieve convergence by the EBCM. Typical examples of our numerical computations are shown in Figs. 6 and 7, where a relative electrical constant of $2.2496 + j0.06$ is assumed [14], which is representative of some maritime aerosols in the near-visible frequency range. The parameters associated with the homogeneous dielectric test cases, as well as the various cross sections of interest are summarized in Table I.

2. TWO-LAYERED SCATTERERS

Since the capability of the GPMT to treat EM scattering from a wide range of homogeneous nonspherical scatterer shapes has been demonstrated, attention is next focused on examining the

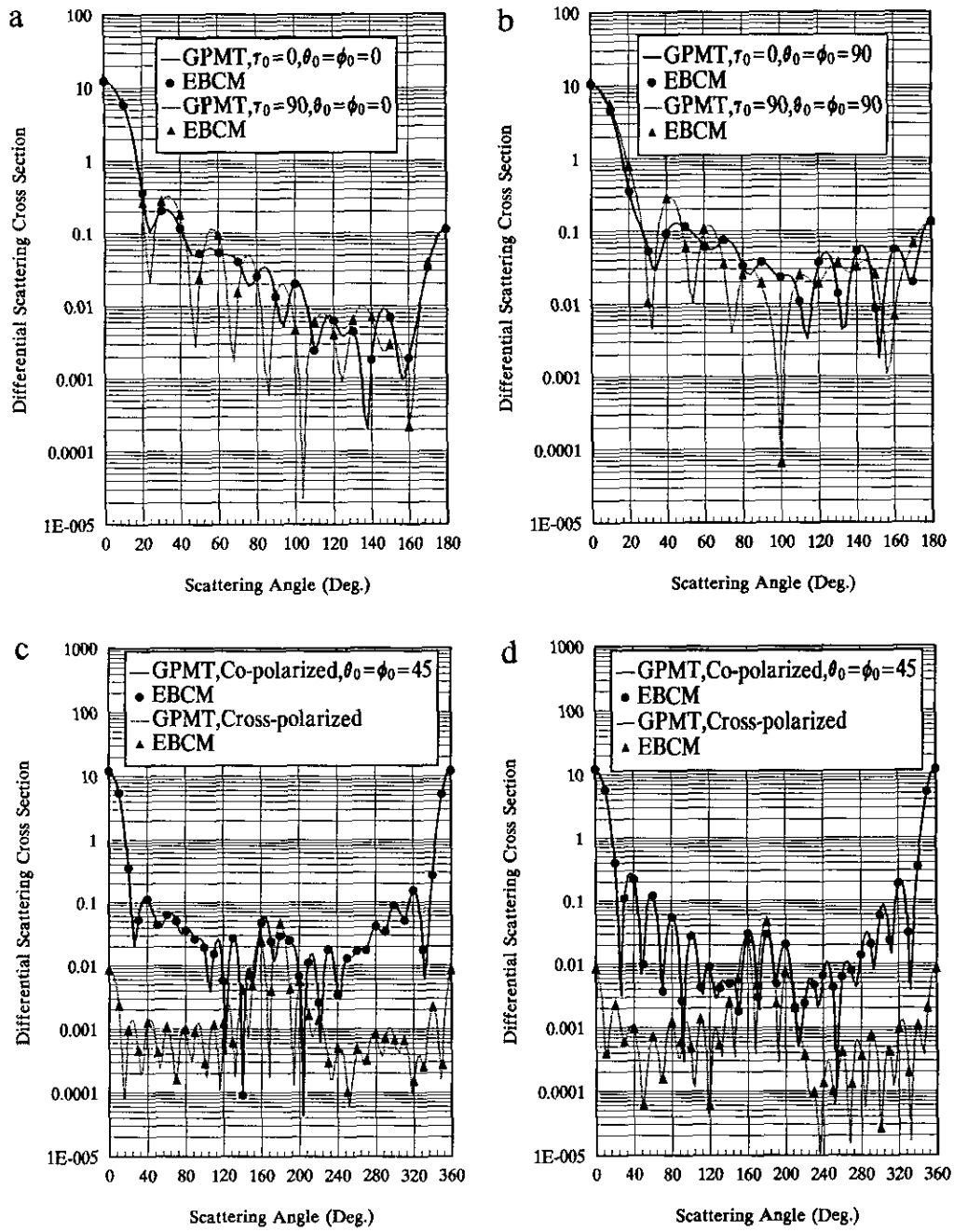

FIG. 6. Plots of normalized differential scattering cross-section patterns for a $T_2(0.1)$ Chebyshev particle with a size parameter of $k_0a_0 = 10$: (c) $\tau_0 = 0°$, main (co-)polarization is parallel to the scattering (xz) plane; (d) $\tau_0 = 90°$, main (co-)polarization is perpendicular to the scattering (xz) plane.

analytical formulations and numerical algorithms developed in [1] specifically for cases involving scattering from rotationally symmetric, PC or dielectric objects, embedded in an axisymmetric dielectric body, which as far as the GPMT is concerned, represents an extension which has neither been developed nor tested so far.

The scattering from concentrically coated spheres with both lossy ($\varepsilon_{r1} = 2 + j1$) and lossless ($\varepsilon_{r1} = 2$) dielectric core materials is considered since there exists an analytical solution via the extended Mie theory [3] for comparison purposes. In all cases to be considered, the size parameter of the outer sphere is fixed at $k_0a_2 = 2$, where a_2 is the radius of the outer sphere, while two values are chosen for the size parameter of the inner sphere, ($k_0a_1 = 0.25$ and 1.8). The coat material is assumed to

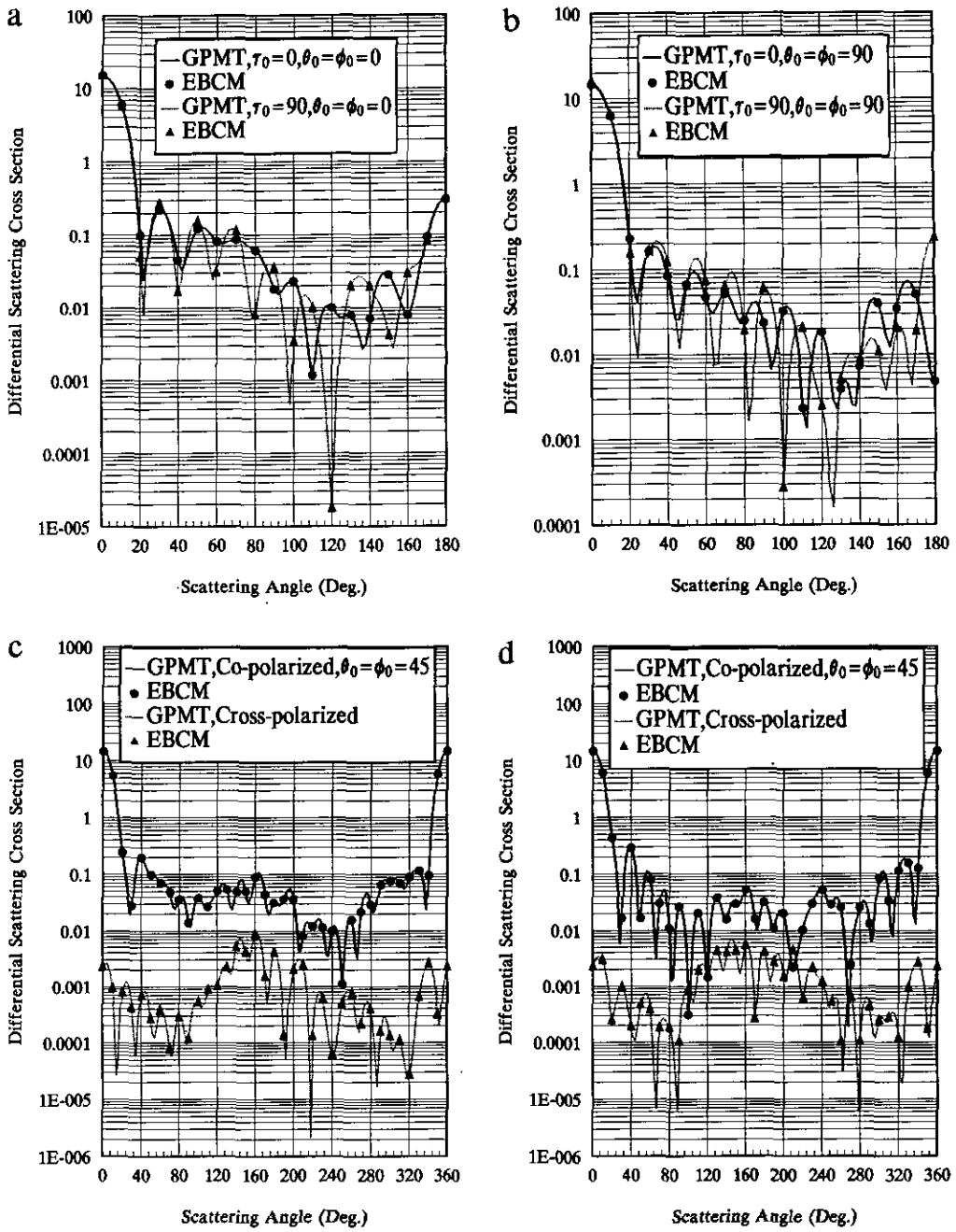

FIG. 7. Plots of normalized differential scattering cross-section patterns for a T_3 (0.1) Chebyshev particle with a size parameter of $k_0a_0 = 10$: (c) $\tau_0 = 0°$, main (co-)polarization is parallel to the scattering (xz) plane; (d) $\tau_0 = 90°$, main (co-)polarization is perpendicular to the scattering (xz) plane.

be either a lossy dielectric with $\varepsilon_{r2} = 4 + j2$ or a lossless one with $\varepsilon_{r2} = 4$. Instead of considering the origin of the local frame to be coincident with the corresponding origin of the principal frame, an assumption which is usually made when this simple geometry is used for testing most of the numerical techniques for inhomogeneous scatterers [16–20], the accuracy of the proposed method will be demonstrated for cases in which displacements of $0.5a_1$ and $0.4a_1$ are assumed for the thick and thin coats, respectively, where a_1 is the radius of the inner sphere. The numerical results for the normalized differential scattering cross-section patterns and the various scattering efficiencies are depicted in Fig. 8 and Table II.

In the following, the GPMT is used to treat EM scattering from an eccentrically stratified PC sphere embedded in a spheri-

TABLE I

Normalized Extinction, Scattering, and Backscattering Cross Sections of the Homogeneous Dielectric Test Cases

Figure	Numerical method	$Q_e/\pi a^2$	$Q_s/\pi a^2$	$Q_b/\pi a^2$
1(a)	Mie theory	2.2181	1.4046	0.3022
	GPMT	2.2176	1.4045	0.3023
1(b)	Mie theory	2.1260	2.1260	6.8353
	GPMT	2.1260	2.1259	6.8388
2	GPMT	4.7615	2.8444	1.0865
	EBCM	4.7616	2.8445	1.0855
3(a)	GPMT	0.5041	0.5019	0.3213
3(b)	GPMT	0.8740	0.8704	0.2109
6(a)	GPMT	2.4743	1.8928	1.4199
	EBCM	2.4743	1.8927	1.4204
6(b)	GPMT	2.3260	1.6511	1.6622
	EBCM	2.3256	1.6511	1.6609
	GPMT	2.2747	1.5936	1.6994
	EBCM	2.2745	1.5937	1.6949
7(a)	GPMT	2.7531	1.9832	3.8194
	EBCM	2.7533	1.9330	3.8238
7(b)	GPMT	2.7912	2.0604	2.9344
	EBCM	2.7913	2.0604	2.9260
	GPMT	2.7032	1.9978	0.0580
	EBCM	2.7032	1.9978	0.0598

cal dielectric coating, a problem which has received comparatively little attention in the literature [16, 21]. Fikioris and Uzunoglu [21] utilized the method of separation of variables while Ström [16] used the EBCM formulation to solve this problem, both in conjunction with the translational addition theorems for the spherical vector wavefunctions, an approach which eventually leads to rather tedious related expressions. In our GPMT approach, the coordinate system is chosen such that the origin of the local frame of the scatterer is fixed at the center of the inner sphere and the z'-axis points in the direction of propagation of the incident wave. Hence, the surface of the outer sphere appears to be nonspherical while the scatterer is rotationally symmetric about the axis of propagation of the incident plane wave.

In Fig. 9 the extinction and backscattering cross sections, normalized by πa^2, where a is the radius of the outer sphere, are presented as functions of the normalized intercenter displacement d/a, where d is the distance between the center of the spheres, $(b/a - 1) \leq d/a \leq (1 - b/a)$ and b is the radius of the inner sphere $\varepsilon_{r2} = 4$, $a/b = 3$ for two size parameters of the outer sphere, $k_0 a = 3$ and 3.375. Two orientations are of the local frame of the scatterer have been considered. In the first, the elevation and aximuthal orientations are $\theta_0 = \phi_0 = 0°$ and hence the scattered electric field vector is always polarized in the same direction of the incident wave, while in the second, $\theta_0 = \phi_0 = 90°$, where two independent polarization vectors are considered as either parallel (in the $\hat{\mathbf{a}}_y$ direction) or perpendicular (in the $\mathbf{a}_x$ direction).

Having verified the validity of the proposed method for scattering from homogeneous as well as concentrically and eccentrically stratified spherical scatterers, attention will next be focused on treating scattering from several arbitrarily shaped axisymmetric dielectric obstacles coated with dielectrics of arbitrary thickness. Numerical results are presented for some selected scatterers since the number of possible combinations is large, depending on the dielectric properties, size and shape of the core and shell regions, as well as on the incidence and polarization directions of the exciting field. Whenever possible, our results are compared against those obtained by an independent numerical method based on the generalization of the EBCM to multilayered nonspherical objects [5], using the single-particle scattering code which has been kindly provided to us by Professor Barber of Clarkson College and others obtained from the RGD approximation [6]. In Figs. 10 through 15 the normalized differential scattering cross-section patterns are shown from some selected two-layered spheroidal objects, the parameters of which are summarized in Table III. In order to satisfy the two basic criteria of the RGD approximation, the relative dielectric constants of the core and coat materials are both assumed to be real ($Q_a^{\parallel,\perp} = 0$) and close to that of the surrounding medium.

As previously mentioned, only cases in which the RGD approximation is valid and/or the EBCM yielded a convergent solution are shown for comparison purposes. Although the numerical results obtained from the EBCM for cases 1 and 4 have been displayed in Figs. 10 and 13, respectively, it should be mentioned that it was eventually impossible to achieve a convergent solution for the differential scattering cross sections over the entire scattering plane, particularly when $\theta_s' = 50°$, 70°, 90°, 100°, 110°, 120°, and 180°. In fact similar problems have been encountered in general for nonspherical scatterers of large size parameters ($k_0 a_2 \geq 6$), in particular when a_1/b_1 (or a_2/b_2) ≥ 2 and/or a_1/b_1 (or a_2/b_2) ≤ 0.6.

As is apparent from the results of these tests, a high degree of agreement has been achieved between the results obtained from GPMT, RGD, and EBCM, with the exception of those cases at scattering angles corresponding to deep nulls, where the effects of accumulated roundoff errors are more noticeable.

Barber and Wang [22] investigated the range of validity of the RGD approximation for homogeneous nonspherical scatterers by performing scattering calculations for a set of arbitrarily as well as randomly oriented prolate spheroids using the EBCM, the results of which were compared to those obtained by the RGD approximation. However, similar comparisons have not yet been made for the case of two-layered nonspherical scatterers. It should be pointed out that, although the maximum errors in the RGD approximation occur at scattering angles corresponding to the deep nulls in the differential scattering pattern (the RGD approximation invariably yields zero for these minima), the positions of these nulls are very well predicted.

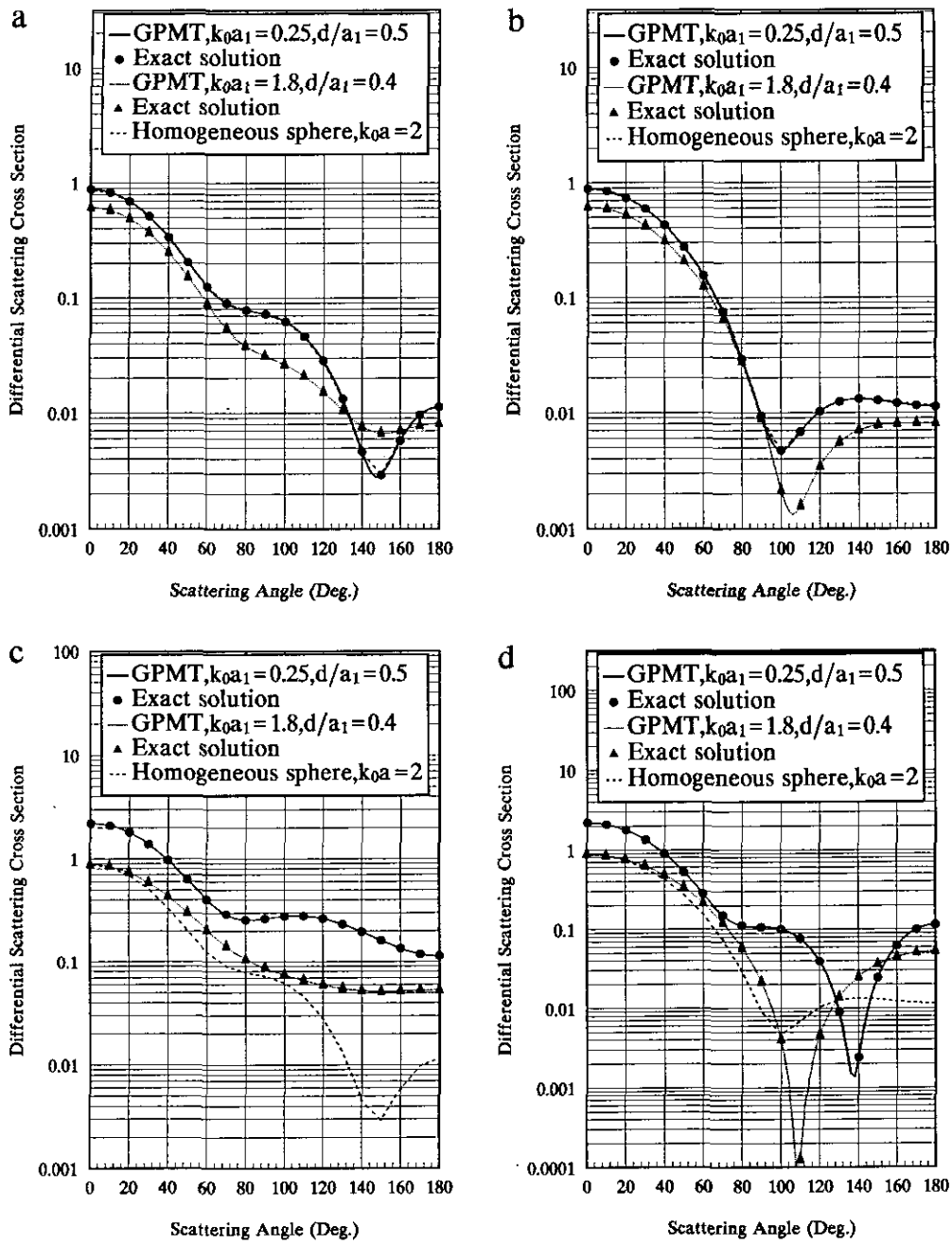

FIG. 8. Plots of normalized differential scattering cross-section patterns for two displaced, concentrically coated dielectric spherical scatterers, $\varepsilon_{1r} = 2 + j1$, $\varepsilon_{2r} = 4 + j2$, $k_0a_2 = 2$: (a) $\tau = 0°$; (b) $\tau = 90°$; $\varepsilon_{1r} = 2$, $\varepsilon_{2r} = 4$, $k_0a_2 \approx 2$: (c) $\tau = 0°$; (d) $\tau = 90°$.

To examine the applicability of the GPMT in the context of two-layered lossy dielectric scatterers, the angular scattering characteristics of partially melted, oblate spheroidal ice-stone models with $a_1/b_1 = a_2/b_2 = 2/3$ and $a_1/b_1 = a_2/b_2 = 0.8$ are shown in Figs. 16 and 17, respectively at a frequency of 3 GHz. Table IV summarizes the parameters associated with the two models, as well as the normalized extinction, scattering, and backscattering cross sections.

It should be pointed out that most of the currently available numerical methods considered either PC obstacles embedded in a dielectric body [17–19] or two-layered lossless dielectric objects [17, 19, 20]. As can be seen from the results of these tests, excellent agreement has been achieved where typical differences between the GPMT and EBCM are less than 1% and thus verifying the validity of the GPMT for predicting the scattering properties of water-coated ice particles not only in

TABLE II

Normalized Extinction, Scattering, and Backscattering Cross Sections of Concentrically Coated Dielectric Spheres

Core region	Coat region	Extended Mie theory				GPMT solution		
		$Q_e/\pi a_2^2$	$Q_s/\pi a_2^2$	$Q_b/\pi a_2^2$	d/a_1	$Q_e/\pi a_2^2$	$Q_s/\pi a_2^2$	$Q_b/\pi a_2^2$
$\varepsilon_{r1} = 2 + j1$ $k_0 a_1 = 0.25$	$\varepsilon_{r2} = 4 + j2$ $k_0 a_2 = 2$	3.2999	1.6448	0.1421	0.5	3.2999	1.6448	0.1421
$\varepsilon_{r1} = 2 + j1$ $k_0 a_1 = 1.8$	$\varepsilon_{r2} = 4 + j2$ $k_0 a_2 = 2$	2.5580	1.1473	0.1018	0.4	2.5585	1.1477	0.1018
$\varepsilon_{r1} = 2$ $k_0 a_1 = 0.25$	$\varepsilon_{r2} = 4$ $k_0 a_2 = 2$	4.7644	4.7644	1.4337	0.5	4.7644	4.7643	1.4338
$\varepsilon_{r2} = 2$ $k_0 a_1 = 1.8$	$\varepsilon_{r2} = 4$ $k_0 a_2 = 2$	2.0756	2.0756	0.6658	0.4	2.0756	2.0756	0.6658

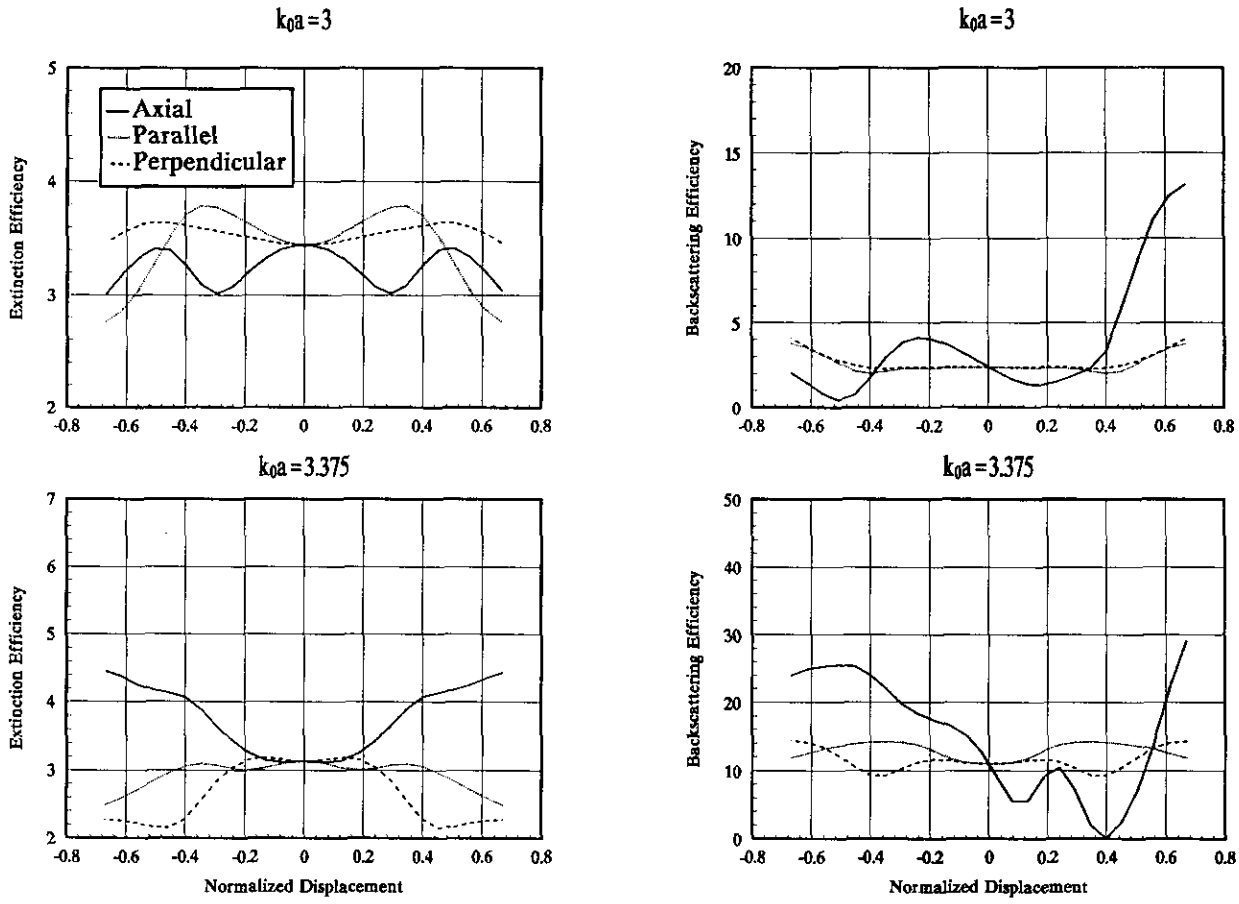

FIG. 9. Normalized extinction and backscattering cross sections of two eccentrically coated, perfectly conducting spherical scatterers as a function of the intercenter displacement, $\varepsilon = 4$, $a/b = 3$, $\theta_0 = \phi_0 = 0$ for axial, $\theta_0 = \phi_0 = 90$ for parallel ($\tau_0 = 90$) and perpendicular ($\tau_0 = 90$) incident polarizations.

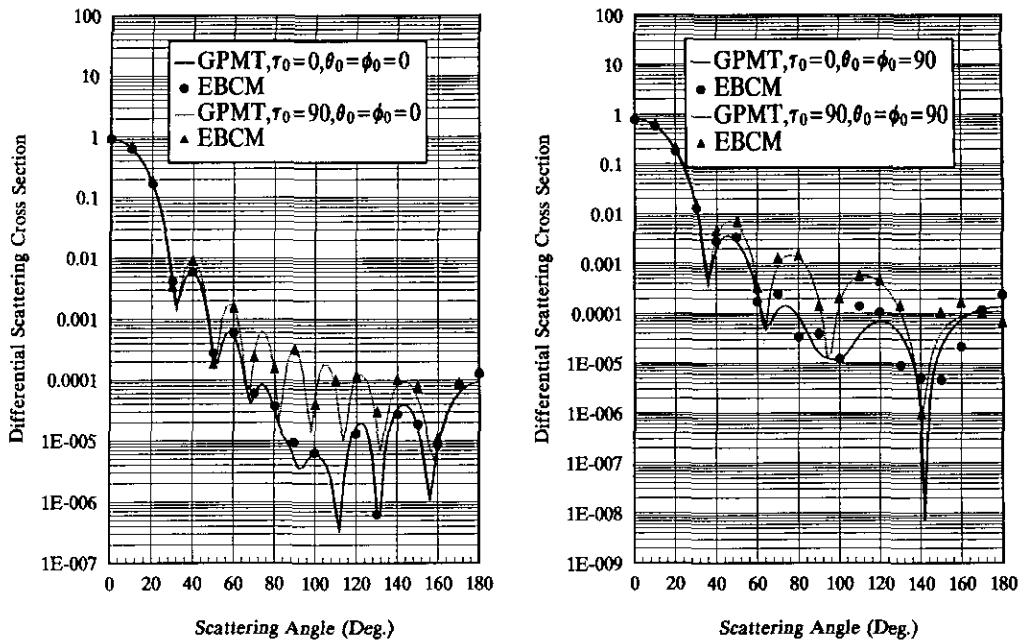

FIG. 10. Plots of normalized differential scattering cross-section patterns for a two-layered object: $a_1/b_1 = a_2/b_2 = 1.88$, $k_0a_1 = 12.5781$m, $\varepsilon_{r1} = 1.092025$, $k_0a_2 = 12.9952$, $\varepsilon_{2r} = 1.205604$.

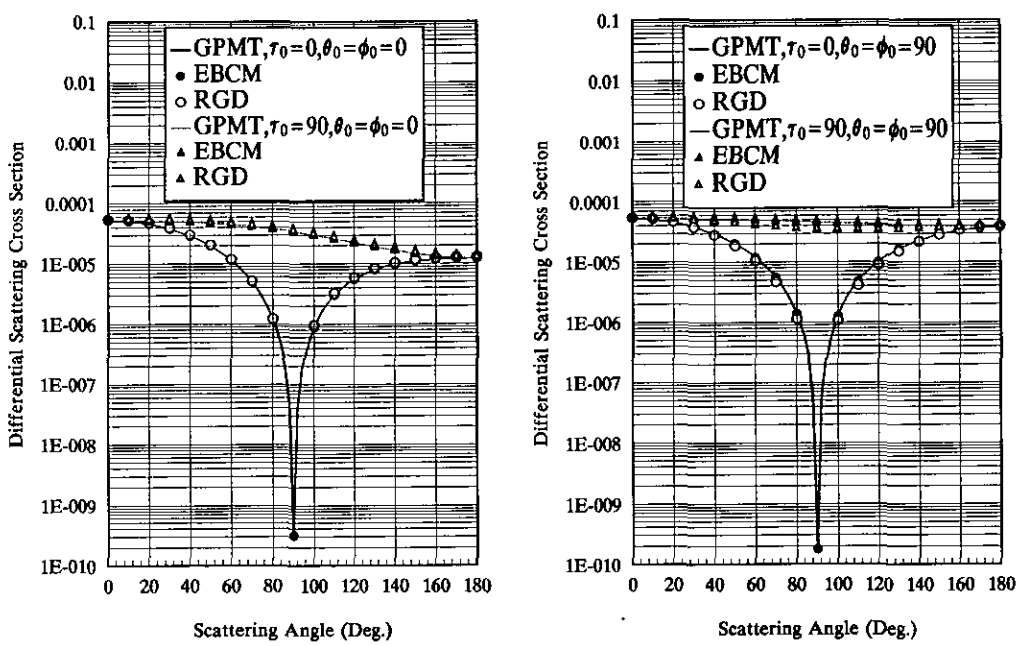

FIG. 11. Plots of normalized differential scattering cross-section patterns for a two-layered object: $a_1/b_1 = a_2/b_2 = 2$, $k_0a_1 = 0.6283$, $\varepsilon_{1r} = 1.0816$, $k_0a_2 = 1.2566$, $\varepsilon_{2r} = 1.1025$.

TABLE III

Normalized Extinction and Backscattering Cross Sections of Two-Layered Spheroidal Biological Models

Figure	Core region	Coat region	θ_0	ϕ_0	τ_0	Numerical method	$Q_e/\pi a_2^2$	$Q_b/\pi a_2^2$
10	$k_0a_1 = 12.5891$	$k_0a_2 = 12.9952$	0°	0°	0°, 90°	GPMT	0.2089	1.2921×10^{-3}
	$a_1/b_1 = 1.88$	$a_2/b_2 = 1.88$				EBCM	0.2092	—
	$\sqrt{\varepsilon_{r1}} = 1.045$	$\sqrt{\varepsilon_{r2}} = 1.098$	90°	90°	90°	GPMT	0.1196	1.4452×10^{-3}
						EBCM	0.1182	—
			90°	90°	0°	GPMT	0.1148	1.6568×10^{-3}
						EBCM	0.1158	—
11	$k_0a_1 = 0.6283$	$k_0a_2 = 1.2566$	0°	0°	0°, 90°	GPMT	2.7998×10^{-4}	1.5265×10^{-4}
	$a_1/b_1 = 2$	$a_2/b_2 = 2$				EBCM	2.7962×10^{-4}	1.5314×10^{-4}
	$\sqrt{\varepsilon_{r1}} = 1.04$	$\sqrt{\varepsilon_{r2}} = 1.05$				RGD	2.8444×10^{-4}	1.6325×10^{-4}
			90°	90°	90°	GPMT	3.6576×10^{-4}	4.8331×10^{-4}
						EBCM	3.7166×10^{-4}	4.9260×10^{-4}
						RGD	3.5753×10^{-4}	4.9681×10^{-4}
			90°	90°	0°	GPMT	3.3674×10^{-4}	4.6825×10^{-4}
						EBCM	3.3599×10^{-4}	4.6647×10^{-4}
						RGD	3.1840×10^{-4}	4.9681×10^{-4}
12	$k_0a_1 = 1$	$k_0a_2 = 2$	0°	0°	0°, 90°	GPMT	4.0311×10^{-3}	2.0203×10^{-5}
	$a_1/b_1 = 2$	$a_2/b_2 = 2$				EBCM	4.0280×10^{-3}	2.1202×10^{-5}
	$\sqrt{\varepsilon_{r1}} = 1.045$	$\sqrt{\varepsilon_{r2}} = 1.098$				RGD	4.0324×10^{-3}	3.3119×10^{-5}
			90°	90°	90°	GPMT	6.4308×10^{-3}	6.5514×10^{-3}
						EBCM	6.4339×10^{-3}	6.5546×10^{-3}
						RGD	5.6967×10	6.5558×10^{-3}
			90°	90°	0°	GPMT	5.0517×10^{-3}	5.7478×10^{-3}
						EBCM	5.0482×10^{-3}	5.7344×10^{-3}
						RGD	4.4182×10^{-3}	6.5558×10^{-3}
13	$k_0a_1 = 5.6548$	$k_0a_2 = 6.2831$	0°	0°	0°, 90°	GPMT	2.4377×10^{-2}	1.9476×10^{-4}
	$a_1/b/1 = 2$	$a_2/b_2 = 2$				EBCM	2.4388×10^{-2}	—
	$\sqrt{\varepsilon_{r1}} = 1.04$	$\sqrt{\varepsilon_{r2}} = 1.05$	90°	90°	90°	GPMT	1.7483×10^{-2}	1.4076×10^{-3}
						EBCM	1.7410×10^{-2}	—
			90°	90°	0°	GPMT	1.5202×10^{-2}	1.4336×10^{-3}
						EBCM	1.5221×10^{-2}	—
14	$k_0a_1 = 0.6283$	$k_0a_2 = 1.2566$	0°	0°	0°, 90°	GPMT	1.1549×10^{-4}	6.2404×10^{5}
	$a_1/b_1 = 2.50$	$a_2/b_2 = 2.5$				EBCM	1.1569×10^{-4}	6.2193×10^{-5}
	$\sqrt{\varepsilon_{r1}} = 1.04$	$\sqrt{\varepsilon_{r2}} = 1.05$				RGD	1.1894×10^{-4}	6.6868×10^{-5}
			90°	90°	90°	GPMT	1.5557×10^{-4}	2.1507×10^{-4}
						EBCM	1.6065×10^{-4}	2.2834×10^{-4}
						RGD	1.5306×10^{-4}	2.2961×10^{-4}
			90°	90°	0°	GPMT	1.4240×10^{-4}	2.1353×10^{-4}
						EBCM	1.4285×10^{-4}	2.1381×10^{-4}
						RGD	1.3554×10^{-4}	2.2961×10^{-4}
15	$k_0a_1 = 1$	$k_0a_2 = 2$	0°	0°	0°, 90°	GPMT	8.2797×10^{-4}	5.8871×10^{-6}
	$a_1/b_1 = 3$	$a_2/b_2 = 3$				EBCM	8.2953×10^{-4}	5.0106×10^{-6}
	$\sqrt{\varepsilon_{r1}} = 1.045$	$\sqrt{\varepsilon_{r2}} = 1.098$				RGD	8.6606×10^{-4}	6.5420×10^{-6}
			90°	90°	90°	GPMT	1.4475×10^{-3}	1.9926×10^{-3}
						EBCM	1.5948×10^{-3}	2.2640×10^{-3}
						RGD	1.3282×10^{-3}	2.1839×10^{-3}
			90°	90°	0°	GPMT	1.1500×10^{-3}	1.8717×10^{-3}
						EBCM	1.1774×10^{-3}	1.9141×10^{-3}
						RGD	1.0207×10^{-3}	2.1839×10^{-3}

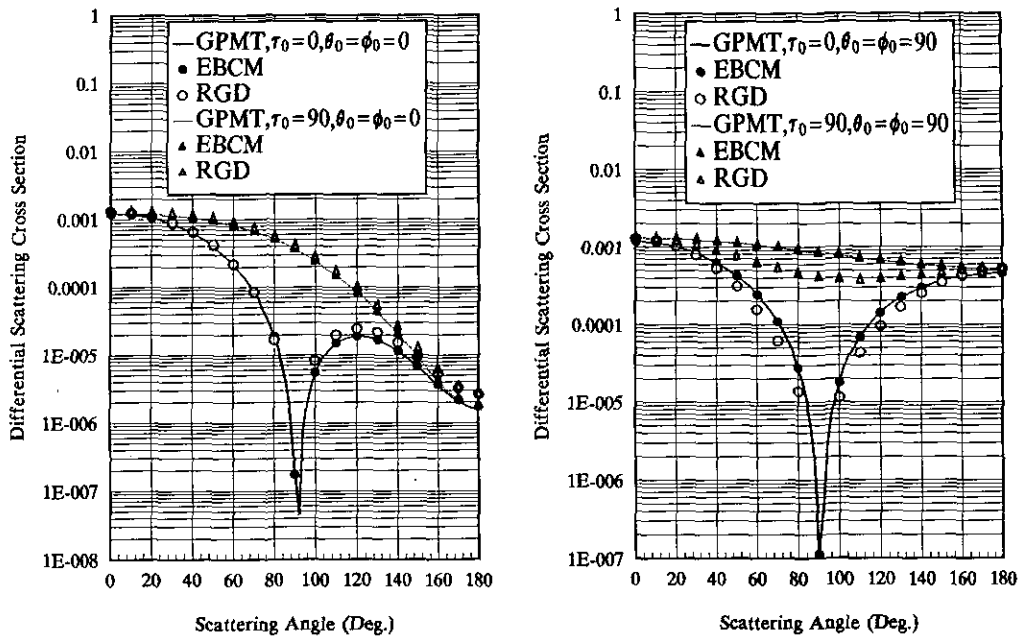

FIG. 12. Plots of normalized differential scattering cross-section patterns for a two-layered object: $a_1/b_1 = a_2/b_2 = 2$, $k_0a_1 = 1$, $\varepsilon_{1r} = 1.092025$, $k_0a_2 = 2$, $\varepsilon_{2r} = 1.205604$.

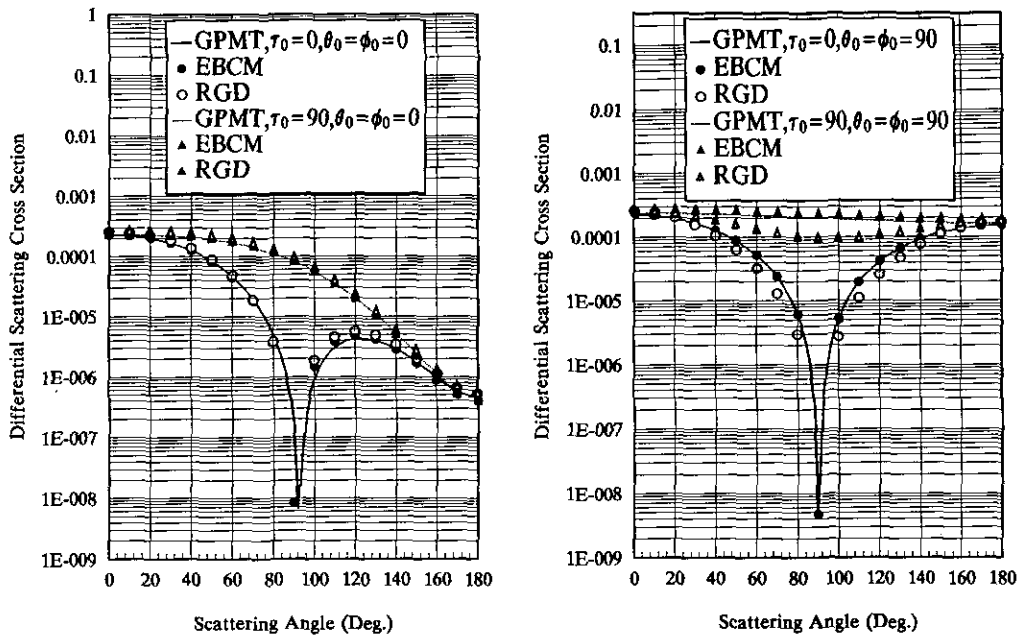

FIG. 13. Plots of normalized differential scattering cross-section patterns for a two-layered object: $a_1/b_1 = a_2/b_2 = 2$, $k_0a_1 = 5.6548$, $\varepsilon_{1r} = 1.0816$, $k_0a_2 = 6.2831$, $\varepsilon_{2r} = 1.1025$.

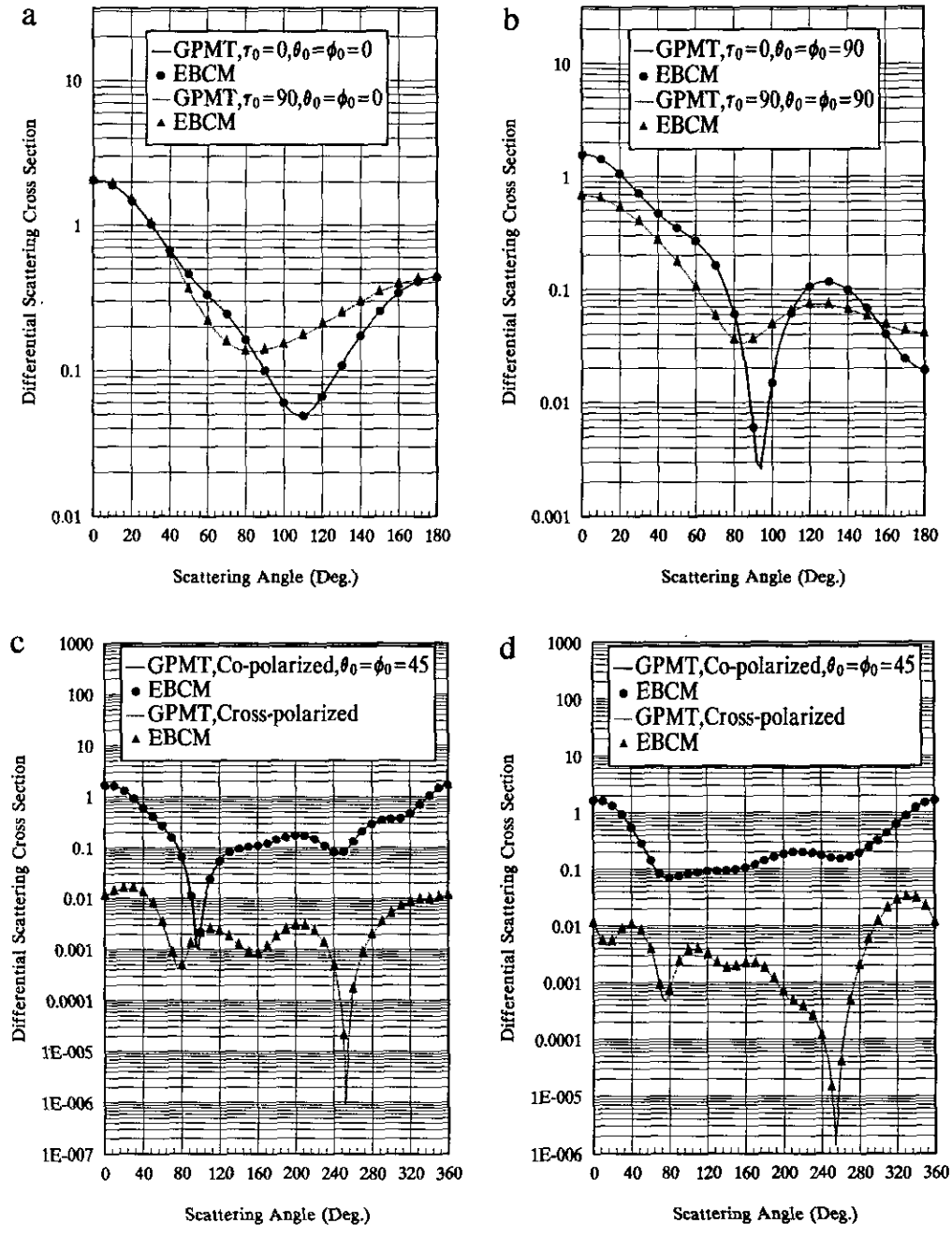

FIG. 14. Plots of normalized differential scattering cross-section patterns for a two-layered object: $a_1/b_1 = a_2/b_2 = 2.5$, $k_0a_1 = 0.6283$, $\varepsilon_{1r} = 1.0816$, $k_0a_2 = 1.2566$, $\varepsilon_{2r} = 1.1025$.

the forward and backward scattering directions, as has been usually the case in the literature [21], but rather over the whole angular scattering pattern.

III. CONCLUSION

This paper has provided several calculations of the differential scattering cross-section patterns and the various cross sections of interest for two orthogonal incident polarization directions of the incident field vector in order to validate the feasibility and applicability of the GPMT as a simple and effective tool for solving a wide class of EM scattering problems. Initially, a number of homogeneous lossy offset spheres, oblate and prolate spheroids, the theoretical raindrop shapes of Pruppacher and Pitter [9], as well as Chebyshev particles [14, 15] were considered. The scattering results thus obtained are com-

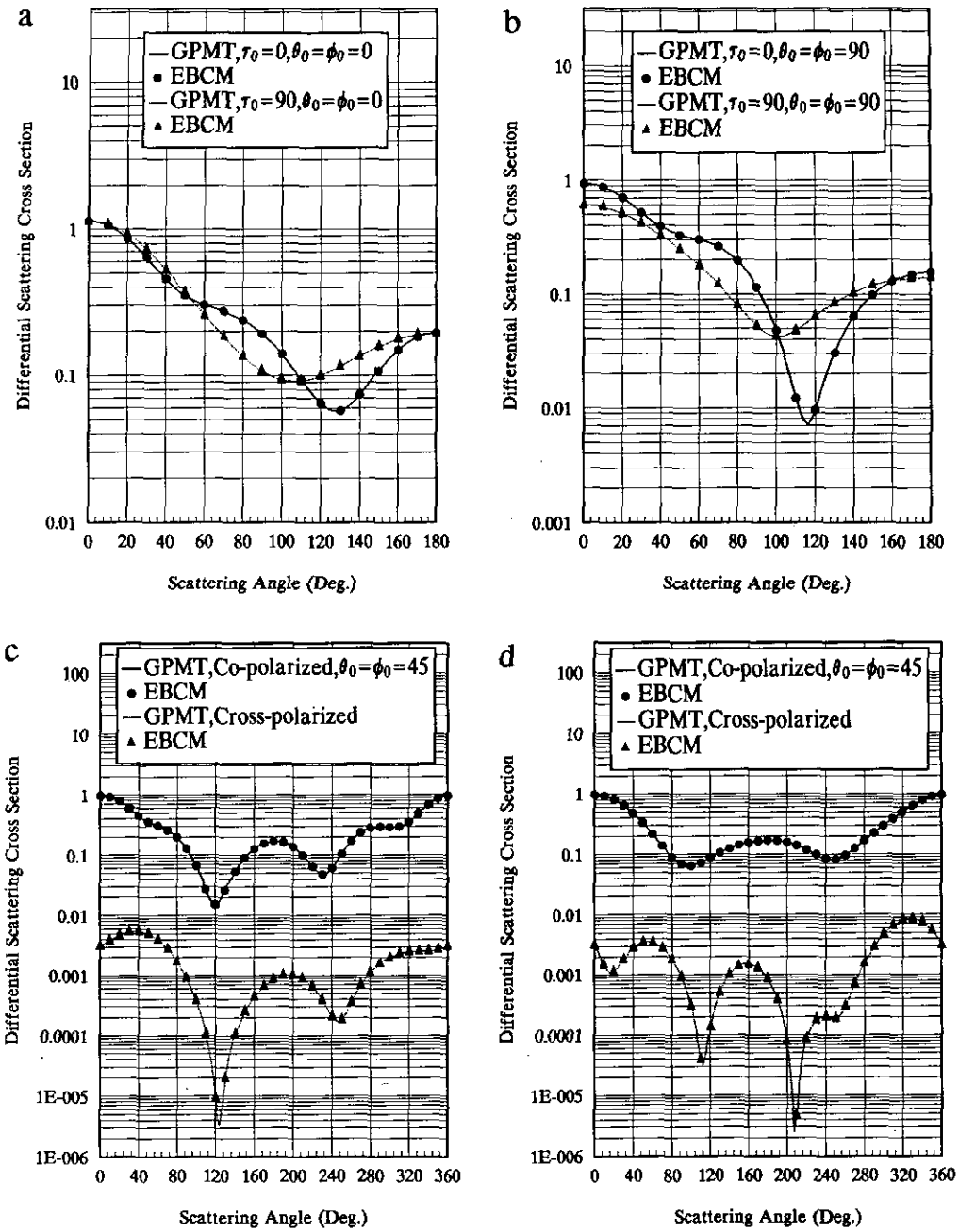

FIG. 15. Plots of normalized differential scattering cross-section patterns for a two-layered object: $a_1/b_1 = a_2/b_2 = 3$, $k_0a_1 = 1$, $\varepsilon_{1r} = 1.092025$, $k_0a_2 = 2$, $\varepsilon_{2r} = 1.205604$.

pared, whenever possible, against those evaluated from the Mie theory [2] and the EBCM [4]. In all of the cases considered, the comparisons of results were surprisingly good, considering the diversity of the methods utilized. As far as scatterer geometries which do not possess a mirror symmetry in the direction of the normal to the axis of revolution are concerned, the homogeneous GPMT was found to be superior to the EBCM, a conclusion which contradicts the claim of Yeh *et al.* [10]. For example, the EBCM was found to be unable to provide a convergent solution over the entire scattering plane for a P-P raindrop with an equivolumic spherical radius of 3.25 mm, even at a frequency of 6 GHz, while the GPMT yielded convergent solutions for all 13 P-P raindrop shapes for frequencies up to at least 200 GHz.

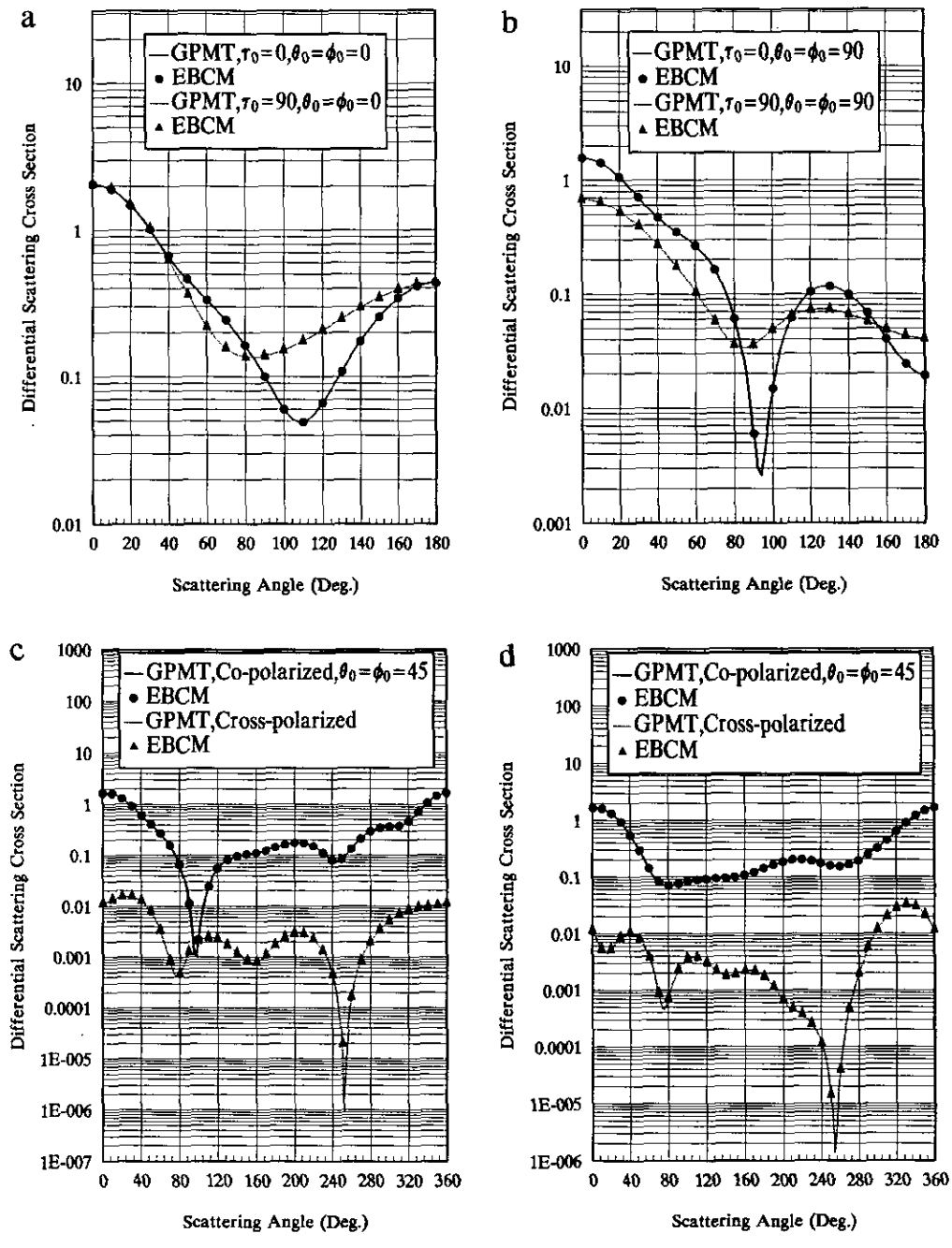

FIG. 16. Plots of normalized differential scattering cross-section patterns of a partially melted, oblate spheroidal hailstone model at a frequency of 3 GHz: $a_1/b_1 = a_2/b_2 = 2/3$, $a_1 = 22.8942$ mm, $a_2 = 30.5257$ mm: (c) $\tau_0 = 0°$, main (co-)polarization is parallel to the scattering (xz) plane; (d) $\tau_0 = 90°$, main (co)polarization is perpendicular to the scattering (xz) plane.

To examine the applicability of the GPMT in the context of rotationally symmetric, PC, or dielectric obstacles embedded in an axisymmetric lossy or lossless dielectric objects, the differential scattering cross-section patterns and the various cross sections have been evaluated for two orthogonal incident polarization directions for many scatterer geometries of practical significance and are presented, starting initially with the preliminary cases of two concentric spheres consisting of different lossy and lossless dielectrics. Excellent agreement has been achieved with the exact solutions [3] and with those obtained from the layered EBCM code [5] and this demonstrates the excellent inherent accuracy and convergence of the GPMT.

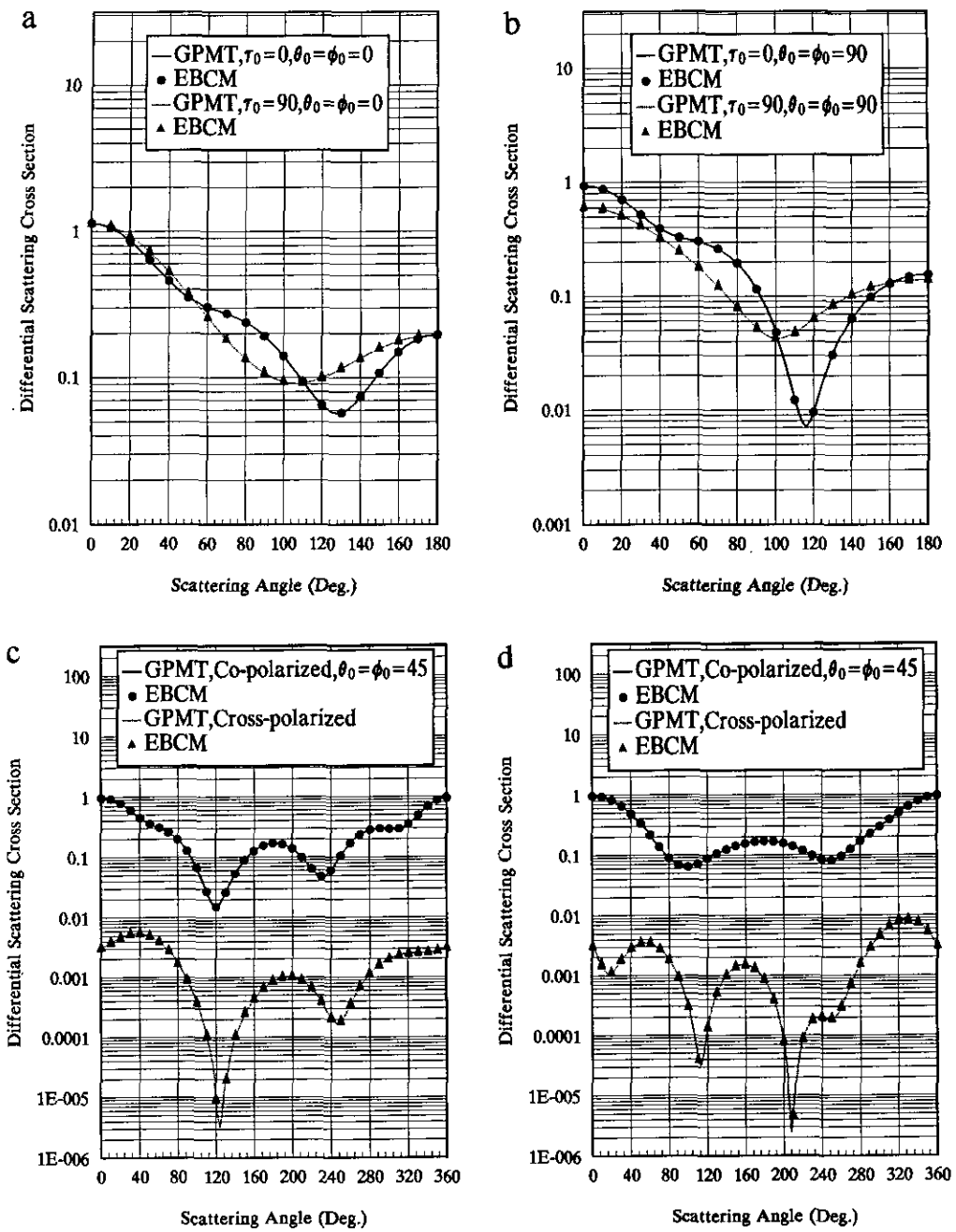

FIG. 17. Plots of normalized differential scattering cross-section patterns of a partially melted, oblate spheroidal hailstone model at a frequency of 3 GHz: $a_1/b_1 = a_2/b_2 = 0.8$, $a_1 = 22.8942$ mm, $a_2 = 30.5257$ mm. $\tau_0 = 0°$, main (co-)polarization is parallel to the scattering (xz) plane; (d) $\tau_0 = 90°$, main (co)polarization is perpendicular to the scattering (xz) plane.

Another important example of the application of the GPMT, which circumvents the use of translational addition theorems for spherical vector harmonics as employed in [16, 21] and, hence, does not require massive analytical and programming efforts while still preserving the computational accuracy and emphasizes the efficiency of the method and its versatility, is the problem of plane EM scattering from an eccentrically stratified PC sphere embedded in a spherical dielectric coating. Finally, the GPMT has been successfully employed to infer the angular scattering patterns of axisymmetric lossy dielectric obstacles coated with lossy dielectrics of arbitrary thickness as models for water-coated, ice-phase hydrometeors.

TABLE IV

Normalized Extinction, Scattering and Backscattering Cross Sections of Partially Melted, Oblate Spheroidal Hailstone Models at a Frequency of 3 GHz

Core	Coat	θ_0	ϕ_0	τ_0	Numerical method	$Q_e/\pi a_2^2$	$Q_s/\pi a_2^2$	$Q_b/\pi a_2^2$
$\frac{a_1}{b_1}=\frac{2}{3}$	$\frac{a_2}{b_2}=\frac{2}{3}$	0°	0°	0°, 90°	GPMT	5.3056	4.1364	5.4901
					EBCM	5.2925	4.1366	5.5058
a_1 = 22.8942 mm	a_2 = 30.5257 mm	90°	90°	90°	GPMT	2.9737	1.9218	0.5136
					EBCM	2.9729	1.9230	0.5130
		90°	90°	0°	GPMT	4.6173	3.2879	0.2454
					EBCM	4.6168	3.2891	0.2428
$\frac{a_1}{b_1}=0.8$	$\frac{a_2}{b_2}=0.8$	0°	0°	0°, 90°	GPMT	3.9337	3.0690	2.4534
					EBCM	3.9345	3.0691	2.4512
a_1 = 22.8942 mm	a_2 = 30.5257 mm	90°	90°	90°	GPMT	2.8406	2.1164	1.7493
					EBCM	2.8397	2.1163	1.7483
		90°	90°	0°	GPMT	3.5762	2.7660	1.9576
					EBCM	3.5759	2.7660	1.9595

REFERENCES

1. H. M. Al-Rizzo and J. M. Tranquilla, *J. Comput. Phys.* **119** (1995).
2. G. Mie, *Ann. Phys.*, **25,** 377 (1908).
3. A. L. Aden and M. Kerker, *J. Appl. Phys.* **22,** 1242 (1951).
4. P. W. Barber and S. C. Hill, *Light Scattering by Particles: Computational Methods* (World Scientific, Singapore, 1990).
5. P. W. Barber, personal communication, 1991.
6. P. J. Wyatt, "Differential Light Scattering Techniques for Microbiology," in *Methods in Microbiology*, Vol. 8, edited by J. R. Norris and D. M. Ribbons (Academic Press, New York/London, 1973), p. 183.
7. P. C. Waterman, *Proc. IEEE* **53,** 805 (1965).
8. M. A. Morgan, *Radio Sci.* **15,** 1109 (1980).
9. H. R. Pruppacher and R. L. Pitter, *J. Atmos. Sci.* **28,** 86 (1971).
10. C. Yeh, R. Woo, J. W. Armstrong, and A. Ishimaru, *Radio Sci.* **17,** 757 (1982).
11. P. C. Waterman, *Alta Freq.* **38,** 348 (1969).
12. P. Barber and C. Yeh, *Appl. Opt.* **41,** 2864 (1975).
13. D. J. Fang and F. J. Lee, *Comsat Tech. Rev.* **8,** 455 (1978).
14. A. Mugani and W. J. Wiscombe, *J. Atmos. Sci.* **37,** 1291 (1980).
15. J. T. Kiehl, M. W. Ko, A. Mugani, and P. Chylek, "Perturbation Approach to Light Scattering by Nonspherical Particles," in *Light Scattering by Irregularly Shaped Particles,* edited by D. Schuerman (Plenum, New York, 1980).
16. Bo. Peterson and S. Ström, *Phys. Rev. D* **180,** 2670 (1974).
17. A. A. Kishk and L. Shafai, *IEE Proc.* **133,** H, 227 (1986).
18. S. M. Rao, C. C. Cha, R. L. Cravey, and D. L. Wilkes, *IEEE Trans. Antennas Propagat.* **39,** 627 (1991).
19. L. N. Medgyesi-Mitschang and C. Eftimitu, *Appl. Phys.* **19,** 275 (1979).
20. D. S. Wang and P. W. Barber, *Appl. Opt.* **18,** 1190 (1979).
21. J. G. Fikioris and N. K. Uzunoglu, *J. Opt. Soc. Am.* **69,** 1359 (1979).
22. P. W. Barber and D. S. Wang, *Appl. Opt.* **17,** 797 (1978).